Electronic Supplementary Information (ESI) for

High capacity carbon dioxide adsorption by inexpensive covalent organic polymers

Hasmukh A. Patel[1], Ferdi Karadas[2], Ali Canlier[1], Joonho Park[1], Erhan Deniz[2], Yousung Jung[1], Mert Atilhan[2*], Cafer T. Yavuz[1*]

[1]*Graduate School of EEWS, Korea Advanced Institute of Science and Technology (KAIST), Daejeon 305-701, Republic of Korea.*

[2]*Department of Chemical Engineering, Qatar University, 2713 Doha, Qatar*

*mert.atilhan@qu.edu.qa, yavuz@kaist.ac.kr

TABLE OF CONTENTS

A. Supplementary Methods

1. Materials

Cyanuric chloride, *N,N*–diisopropylethylamine (DIPEA), piperazine (anhydrous), 4,4'–bipiperidine were purchased from Sigma-Aldrich, USA. 1,4-dioxane, toluene, dimethyl acetamide, THF and ethyl alcohol were purchased from SAMCHUN, South Korea. All chemicals were used as received except 1,4-dioxane where molecular sieves were used to dry the stock solvent.

2. Synthesis of COP-1

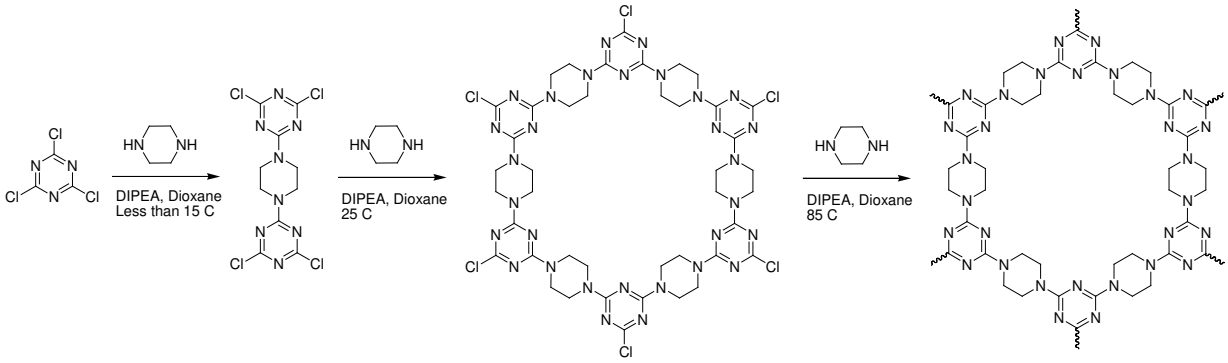

DIPEA (18.9 mL, 108.4 mmol) was added to piperazine (3.73 g, 43.3 mmol) dissolved in 1,4-dioxane (150 mL) at 288 K. Cyanuric chloride (5.00 g, 27.1 mmol) dissolved in 1,4-dioxane (50 mL) was added dropwise to the above solution with continuous stirring at 15 ^{o}C in an N_2 environment. The white precipitate was stirred at 15 °C for 1 h, before being stirred at 25 ^{o}C for 2 h and then at 85 ^{o}C for 21 h. The off-white precipitate was washed with 1,4-dioxane and soaked in EtOH three times over the period of 12 h. Finally, the precipitate was dried at room temperature under vacuum for 2 h. This sample was designated as COP-1.

3. Synthesis of COP-2

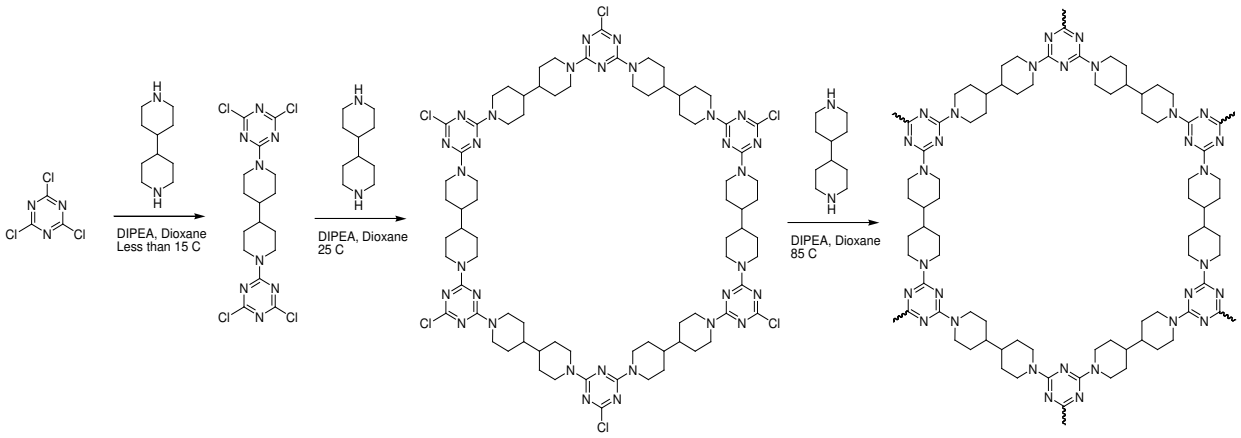

DIPEA (1.5 mL, 8.6 mmol) was added to 4,4'-bipiperidine (0.46 g, 2.7 mmol) dissolved in 1,4-dioxane (80 mL) at 15 °C. Cyanuric chloride (0.30 g, 1.6 mmol) dissolved in 1,4-dioxane (10 mL) was added dropwise to the above solution with continuous stirring at 15 °C in an N_2 environment. The white precipitate was stirred at 15 °C for 1 h, before being stirred at 25 ^{o}C for 2 h and then at 85 ^{o}C for 21 h. The white precipitate was washed with 1,4-dioxane and soaked in EtOH three times over the period of 12 h. Finally, the precipitate was dried at room temperature under vacuum for 2 h. This sample is designated as COP-2.

4. Characterisation

CHNS analyses were performed on elemental analyser ThermoQuest Italia S.P.A (CE instrument). FT-IR spectra were recorded as KBr pellet using a Perkin-Elmer FT–IR spectrometer. ^{1}H and ^{13}C NMR spectra were recorded on a Bruker DMX400 NMR spectrometer. Solid-state cross polarization magic angle spinning (CP/MAS) NMR spectra were recorded on a Bruker Anence III 400 WB NMR spectrometer. Thermogravimetric analysis (TGA) was

performed on a NETZSCH-TG 209 F3 instrument by heating the samples to 800 °C at 10 °C.min^{-1} in N_2 or air atmosphere. N_2 sorption isotherms were obtained with a Micromeritics ASAP 2020 accelerated surface area and porosimetry analyser at 77 K. Prior to analysis, the samples were degassed at 150 °C for 5 h under vacuum. The adsorption-desorption isotherms were evaluated to give the pore parameters, including BET surface area, pore size, and pore volume. X-ray diffraction (XRD) patterns of the samples were acquired from 0.5 to 60° by a Rigaku D/MAX-2500 (18kW) Micro area X-ray diffractometer.

5. Theoretical Simulations

Theoretical CO_2 capture capacities were determined by Cerius2 v. 4.0 software (Accelrys Software Inc., San Diego, CA, USA). The force field (FF) parameters and charges for CO_2 were adapted from J. G. Harris et al.[1], and for COP-1 from Dreiding2.21 and the equilibrium charge method in Cerius2. The amorphous polymer frame of COP-1 was prepared by using a building module in Cerius2. To calculate the available volume, the probe radius 1.4 Å was used.

B. Supplementary Discussion

Covalent organic polymers (COPs), made from cyanuric chloride (CC, 2,4,6-trichloro-1,3,5-triazine) and an appropriate organic linker (Fig. S1), feature microporosities which display modest to significant gas sorption properties. In order to verify the chemical compositions of the COPs, we carried out theoretical calculations and a number of chemical analyses.

For a ***theoretical*** understanding of CO_2 uptake capacity in the amorphous polymer COP-1 several structures were tested depending on the reaction conditions and stoichiometry since the polymer superstructure is largely unknown. The CC has three binding sites and piperazine has two. In one extreme, they can make 1-dimensional chain-like network with a 1:1 reaction ratio. But in the other extreme, they can form a planar structure with 2:3 (CC:piperazine) reaction ratio where all the binding sites of CC and piperazine are occupied by each other, making an imaginary crystalline COP-1. In the practical amorphous COP-1 these two extreme structures could be mixed. The present force field cannot perfectly reproduce the experimental values, especially at high pressure (Figure 1) where the available volume is more important than CO_2 affinity in the performance of sorbents for CO_2 capacity. In amorphous COP-1, there is a large void which can contain CO_2 in voluminous scale with its porosity of 85 % (6.7 cm^3/g) and density of 0.127 g/cm^3 which makes amorphous COP-1 the best material for CO_2 capture at high pressures (Figure 1 and Fig. S3). The CO_2 affinity of amorphous COP-1 of course also plays a role to store gas on its surface. In low pressures, the CO_2 molecules are attracted to the inner polymer surface, rather than distributed randomly in the unit cell as can be shown in a movie clip (Movies S1-S2).

^{13}C- NMR and ^{1}H-NMR spectra with the assignment of the chemical shifts are shown in Fig. S4. The presence of aliphatic CH_2 group was confirmed from the ^{13}C chemical shift at 44.2

and 43 ppm for COP-1 and COP-2, respectively. The CH functionality in COP-2 shows another, but lower ^{13}C chemical shift at 29.3 ppm. The triazine ring carbons were assigned to 164.7, 164.3 and 180.6 ppm, in the ^{13}C NMR spectra of COP-1 and COP-2, respectively. In the case of the ***^{1}H-NMR spectra***, chemical shifts at 3.2 ppm correspond to methylene groups of piperazine and bipiperidine in COP-1 and COP-2, respectively. The broad chemical shift in COP-2 can be attributed to the diverse interactions between CH and CH_2 groups of bipiperidine. Internal standard TMS shows the reference chemical shift at 0 ppm.

Functional groups present in COPs show characteristic FT-IR absorptions. In their respective ***FT-IR spectra***, several strong bands in the 1200-1600 cm^{-1} region were identified corresponding to the typical stretching modes of CN heterocycles (Fig. S5). Additionally, the characteristic breathing mode of the triazine units is evident around 800 cm^{-1}. The absorption band of saturated carbons of piperazine and 4,4' -bipiperidine are assigned near 2930 cm^{-1}. The absence of the characteristic C–Cl stretching vibration at 850 cm^{-1} confirmed that all three chlorine atoms on CC have been substituted.

Solvents are known to have direct impact [3] on the porosity of microporous polymers. Dioxane and THF are commonly chosen as solvents in cyanuric acid based reactions [4] on account of their inert behavior towards the CC and linkers. Since the substitution of all three chlorides with the linkers used in this investigation was not possible below 85 °C, THF was found to be ineffective since its boiling point is 68 °C. Dimethyl acetamide, toluene and ethanol all react with cyanuric chloride, restricting the interaction of linkers and results in low surface area products. Table S1 shows the solvent effect on the surface area of COP-1.

In order to find out about the ***porosity of COP structures***, nitrogen adsorption isotherms were obtained with a Micromeritics ASAP 2020 accelerated surface area and porosimetry

analyser at 77 K after the samples were degassed at 150 °C for 5 h under vacuum. The adsorption-desorption isotherms were evaluated to give the pore parameters (Table S4), including ***Brunauer-Emmett-Teller (BET)*** and ***Langmuir surface area***, pore size and pore volume. The micropore surface area was determined by the *t* method. The slope of the *t*-plot is directly proportional to the surface area of the sample. Any upward deviation from linearity is a result of the capillary condensation inside the pores and the initial slope is proportional to the micropore surface area.

The ***low pressure CO_2 and N_2 adsorption-desorption*** isotherms (Figure 3) for COPs were measured at 273 K using a static volumetric system (ASAP 2020, Micromeritics Inc., USA). The temperature during adsorption and desorption was kept constant using a circulator. Prior to adsorption measurements, the samples were dried at 373K for 24 h. The samples were further activated in situ by increasing the temperature at a heating rate of 1 K min^{-1} up to 423 K under vacuum (5×10^{-3} mmHg) and the temperature and vacuum was maintained for 5 h before the sorption measurements.

The selectivity of CO_2 over N_2 and total CO_2 adsorption per surface area is tabulated for all COPs in Table S5. Powder ***X-ray diffraction (XRD)*** patterns (Fig. S6) of the COPs were acquired from 0.5 to 60° by a Rigaku D/MAX-2500 (18kW) Micro area X-ray diffractometer. No crystallinity was observed, as expected from the CO_2 capacity simulations (Figure 1).

Thermal and water stability of an adsorbent is of prime value when it is planned to be utilized for adsorption of carbon dioxide evolved from a fossil fuel burning thermal power plant. COPs synthesized in this work have been subjected to extreme moist conditions at boiling temperatures to study the stability in steam-like gas streams.

Thermogravimetric analyses of COP-1 and COP-2 were performed up to 800 °C at a heating rate of 10 °C.min^{-1} in air and N_2 environment (Figure 4 and Fig. S1). COP-1 and COP-2 started to decompose at 285 and 290 °C, respectively, in air and 360 and 362 °C in dinitrogen atmosphere, verifying their potential in the given range of CO_2 scrubbing operations (0–180 ^{o}C, see the main text).

For a reliable ***water stability*** test, 100−300 mg of COP-1 and COP-2 were dispersed in H_2O (15 mL) and kept at 100 °C for 1 day, 3 days and 1 week. Samples were drawn after specified time periods, filtered and dried at 100 °C. Their respective surface areas (77 K, Figure 4) and CO_2 adsorptions (273 K and 1bar, Figure 4) were measured. In the case of all samples, COP-1 and COP-2 showed no significant loss of surface areas or CO_2 capacities, proving their robust nature.

Industrially relevant pressure ranges (0−175 bar, see the main text) dictate the necessity of high pressure gas adsorption measurements. Though it is relatively insignificant at low pressures, ***density*** becomes a crucial component of capacity calculations because of the compression of the guest molecules inside the pores of the materials. For many recently developed porous materials, especially for high surface area materials (MOFs, COFs and porous polymers), crystal density have been utilized for their high pressure adsorption studies. Since crystal density ignores the inter-particle voids, bulk density or tapped bulk densities are required in order to assess their viability in industrial processes. In a typical analysis, ***bulk density measurements*** are carried out with the corresponding material filling a 5 mL cylinder. The ratio of weight-to-volume gives bulk density (Table S2). In a ***tapped bulk density measurement***, COPs were filled in a 5 mL cylinder before being tapped vertically 100 times and the volume

and weight noted. The ratio of weight to volume gave the tapped bulk density. It was noted that the volume of the material in cylinder was not changed substantially after 75 tappings.

High pressure hydrogen adsorption measurements at 298 K up to 100 bar were carried out in an automated high pressure gas adsorption system BELSORP-HP, BEL Japan, Inc. Prior to the sorption isotherm measurements, samples were activated at a heating rate of 1 K min^{-1}, to 423 K under vacuum (6.7×10^{-2} Pa). The temperature and vacuum was maintained for 6 h before the sorption measurements. After activation, samples were allowed to cool down to 298 K. The amount of activated sample was determined from the weight of sample before and after activation. H_2 adsorption–desorption studies at 298 K (Table S7) were performed by maintaining the temperature using an external water circulator (Poly Science, USA).

For ***high pressure*** (up to 200 bar) ***CO_2 sorption measurements***, a Rubotherm® magnetic suspension sorption apparatus (Fig. S7-S8, Tables S8-10 and www.rubotherm.de) based on magnetic levitation was employed. The magnetic suspension balances make it possible to weigh the samples of interest in almost all environments including compressed gas at high pressures and high temperatures with a balance located at ambient conditions. The sample is located in the measuring cell and can be coupled specifically to the balance without a physical link. An electromagnet, which is attached to the bottom of the balance, lifts a so-called suspension permanent magnet assembly (PMA) that consists of a permanent magnet, sensor core and a measuring load basket (or cage). The electromagnet assembly (EMA), which is attached to the bottom of the weighing balance via hook connections, maintains a free suspension state of the PMA via an electronic control unit. This arrangement allows different vertical positions for the PMA based on the control action commands to the EMA. The first position is called the zero

point (ZP) in which the suspension part suspends alone contactless and thus represents the unburdened balance. The second EMA point is called the measuring point (MP) in which the suspension part reaches to a higher vertical position and couples the sample to the balance and transmits the weight of the sample to the balance. This principle is illustrated in the Fig. S9.

For buoyancy calculations used in sorption measurements, in-situ density of the pressurized gas in the high-pressure cell is measured. Archimedes' principle is used for density measurements by utilizing a calibrated silicon sinker placed just above the sample basket in the pressure cell. The silicon sinker used in this apparatus had a volume of 4.4474 cm^3 measured at 20 ^0C with a 0.0015 cm^3 uncertainty and a density of 4508 kg/m^3 measured at 20 ^0C with a 4 kg/m^3 uncertainty.

Buoyancy force on a submerged object is famously explained by Archimedes' principle: "when a solid body (sinker) is immersed in a fluid, it displaces a volume of fluid the weight of which is equal to the buoyancy force exerted by the fluid on the sinker." Magnetic sorption apparatus is equipped with a sinker body, which enables the in-situ density measurements of the adsorbate gas based on Archimedes' hydrostatic buoyancy method via contactless magnetic levitation principles. In classical buoyancy based densimeters, a sphere or cyclinder shaped sinker hangs from a commercial digital balance by a thin wire. The pressure and temperature of the fluid remains constant in the pressure cell using a temperature control mechanism. The sinker is submerged in the fluid, and the weight of the sinker is measured. According to the same Archimedes' principle, the density of the fluid is:

$$\rho = \frac{m_v - m_a}{V_s(T,P)} \qquad (1)$$

In Eq 1, m_v is the 'true' mass of the sinker measured in vacuum, m_a is the apparent mass of the sinker in the fluid that is charged in the pressure cell and V_s is the calibrated volume of the sinker, which is a function of temperature and pressure [5]. When compared with the classical buoyancy densimeters, the novelty of the magnetic suspension coupling is that it uses non-physical-contact force transmission between the sinker in the pressurized cell and the weighing balance at atmospheric pressure, thus allowing a cell design that covers wide temperature and pressure ranges [6].

In a typical sorption measurement, the weight of the adsorbent is measured initially under vacuum and that is followed by weight measurements of the adsorbent at each pressurized adsorbate gas condition. Meanwhile a titanium sinker with a calibrated volume is weighed continuously in a sequential order with the sorption measurements in order to obtain the density of the measuring fluid surrounding the sample as it is required for the buoyancy correction of the measured sorption values. The simultaneous measurement of sorption and density is especially needed if the buoyancy effects caused by the density of the adsorbate gas are large, i.e., high pressure or low temperature conditions. From thermodynamics point of view, density measurement in a binary gas mixture also offers the possibility of determining the concentration for the gas mixture without further analysis since the density is a function of the mixture composition.

Typical measurements start with placing an approximately 0.25 g of a sorbent sample within the sample holder after activating by degassing at 150 ^{o}C. Once the sample is in place, the system is taken under vacuum for 24 h at 65 ^{o}C. Carbon dioxide is then pressurized via a Teldyne Isco 260D fully automated gas booster and charged into the high-pressure cell. For each pressure point it takes about 45 minutes to reach equilibrium and once temperature and pressure

equilibrium is reached, four different sets of measurements are taken for a period of 10 min each. During the 10 min measurement period pressure, temperature and weighing measurements are collected at every 30 sec along with the sinker weight measurements for in-situ density values of the absorbate gas. Some pressure points might require repetition, depending on the experimental stability. Consequently, the total duration of each experimental sorption measurement takes about 40 to 60 min. At the end of each pressure point, the system goes to the next automatically.

In this work, pressures up to 200 bar are used for maximum pressure and at the end of each isotherm, a hysteresis check is conducted by collecting desorption data as the system is depressurized. The temperature of the high-pressure cell is controlled by an automated external constant temperature circulator (Polyscience model 9512) via a platinum resistance thermometer (Jumo DMM 5017 Pt100) attached to the high-pressure cell body. The cell temperature is maintained within ± 0.6 °C accuracy. The automatic gas dosing system is used for controlling the pressure inside the high-pressure cell. The pressure control unit is a combination of shut valves, a special PID control instrument and precise pressure transducer, Paroscientific® Digiquartz 745-3K with an accuracy of with an accuracy of 0.01 %. The schematic of the automatic gas dosing system is given in Fig. S10.

Adsorption data is analyzed and the amount of adsorbed gas on the sample is calculated by using the equation below:

$$W + W_{buoy\,,sample} + W_{buoy\,,sink} = m_{ads} + m_{sample} + m_{sink} \qquad (2)$$

where;

W = Signal read by the instrument

$W_{buoy\ ,sample}$ = V_{sample}*d_{gas} = Buoyancy correction due to the sample

V_{sample} = Volume of the sample

$V_{sample} = V_{total} - V_{pore}$

d_{gas} = Density of the gas

$W_{buoy\ ,sink} = V_{sinker} * d_{gas}$ = Buoyancy correction due to the sinker

V_{sinker} = Volume of the sinker

m_{ads} = Surface excess mass of the CO_2

m_{sample} = Mass of the sample

m_{sink} = Mass of the sinker

d_{gas} is measured *in situ* and the mass of empty sinker is measured at several pressures of helium to determine the buoyancy caused by the sinker ($W_{buoy,sink}$). Volume of the sinker (V_{sinker}) is calculated from the slope of weight vs. density plot obtained from this measurement. A blank measurement at vacuum is performed to determine the mass of the sinker (m_{sink}). The buoyancy correction caused by the sample ($W_{buoy,sample}$) is performed by calculating the volume of the sample (V_{sample}), which is obtained by subtracting the pore volume of the sample measured by BET analysis (V_{pore}) from the total volume of the sample (V_{total}) calculated from the density of the material determined by tapping method (Table S2). A typical screenshot from the sorption apparatus for vacuum measurement and adsorption test under pressure measurement is given in Fig. S11.

The single-sinker densitometer also operates based upon Archimedes' principle for the buoyancy force acting on a cylindrical sinker in the presence of a fluid. The density is calculated by measuring m_v, the 'true mass' of the sinker in vacuum, m_a, the 'apparent mass' of the sinker in the presence of fluid and v_S, the volume of the sinker:

$$\rho = \frac{m_v - m_a}{v_S} \tag{3}$$

The sinker volume appearing in above equation undergoes a change because of distortion of the sinker material at a temperature and pressure (T, P) other than the reference temperature and pressure (T_o, P_o) at which the reference sinker volume, v_{So}, is measured.

$$v_S(T,P) = v_{So}(T_o,P_o) + v_{So}(T_o,P_o)\left[3\frac{\Delta L}{L_o}(T) - 3\frac{(P-P_o)}{E(T)}\{1-2\upsilon(T)\}\right] \tag{4}$$

where, $\Delta L/L_o$ is the thermal expansion, E is the Young's modulus and υ is the Poisson's ratio of the sinker material at a temperature, T. The thermal expansion was calculated using:

$$\frac{\Delta L}{L_o}(T) = \alpha(T - T_o) \tag{5}$$

where, α is the thermal coefficient of expansion of the sinker material. For titanium, α is calculated to be 8.8×10^{-6} K^{-1} in the range (-80 to 260) ^oC. The reference sinker volume calibration, Rubotherm made the measurements at 20 ^oC and 990.4 mbar as 4.4474 cm^3 with the uncertainty of 0.0015 cm^3 in sinker volume.

C. Supplementary Figures and Movies

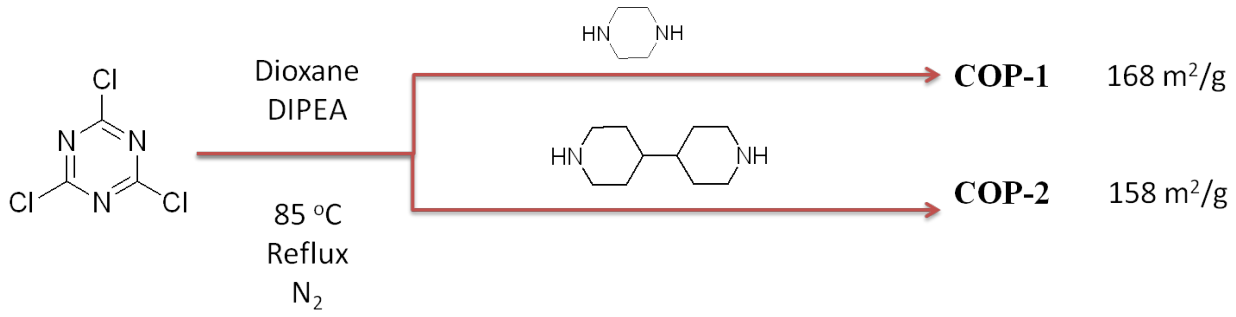

Fig. S1. Summary of the COPs synthesized in this study and their corresponding BET surface areas. COPs synthesized using CC as the core and organic linkers to extend into structural frameworks.

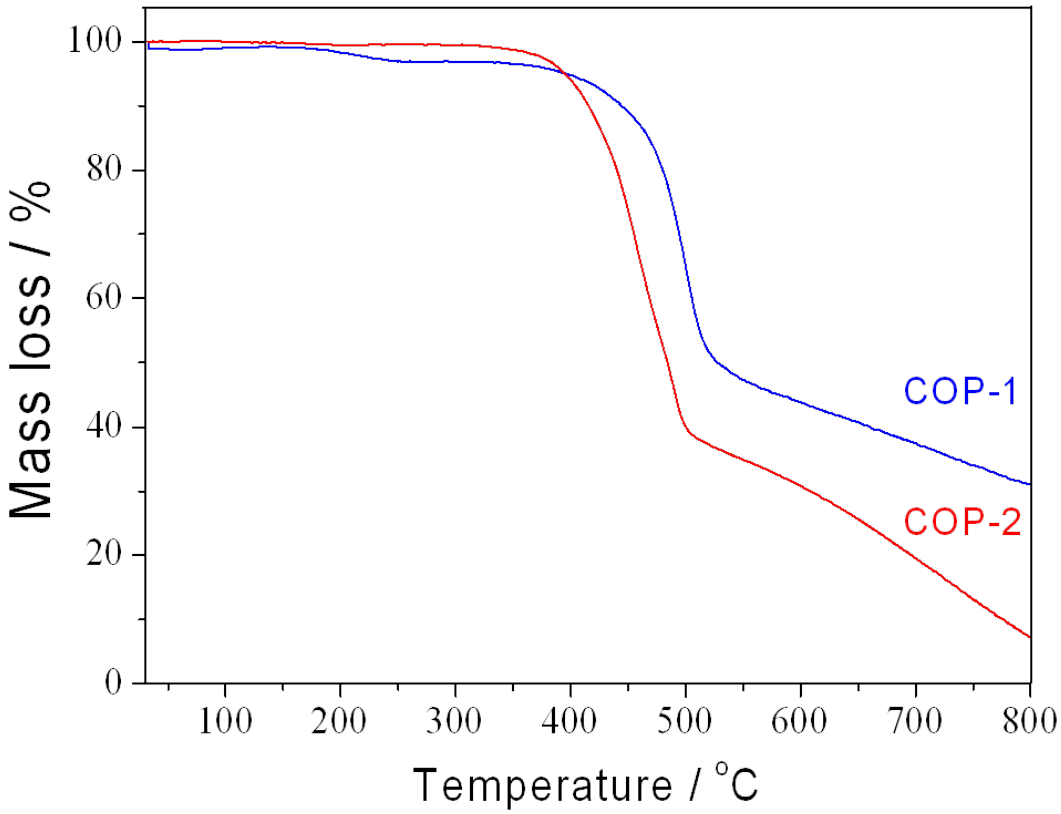

Fig. S2. Thermogravimetric analysis of COP-1 and COP-2 in dinitrogen environment.

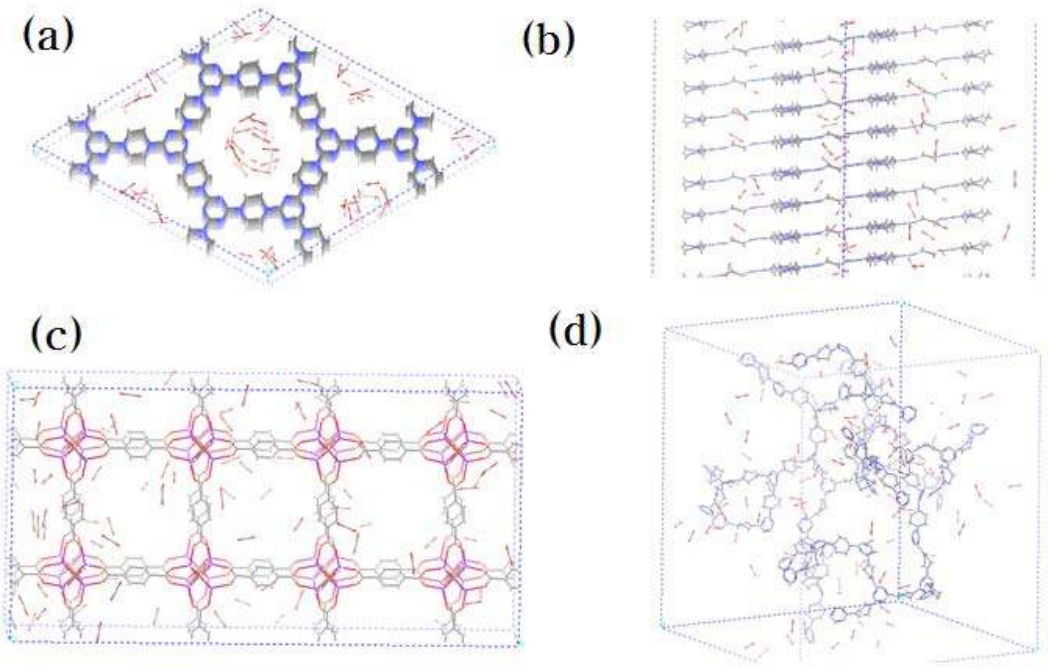

Fig. S3. The CO_2 capture profiles in crystalline COP-1 (**a**) top and (**b**) side view, (**c**) MOF-5, and (**d**) amorphous COP-1.

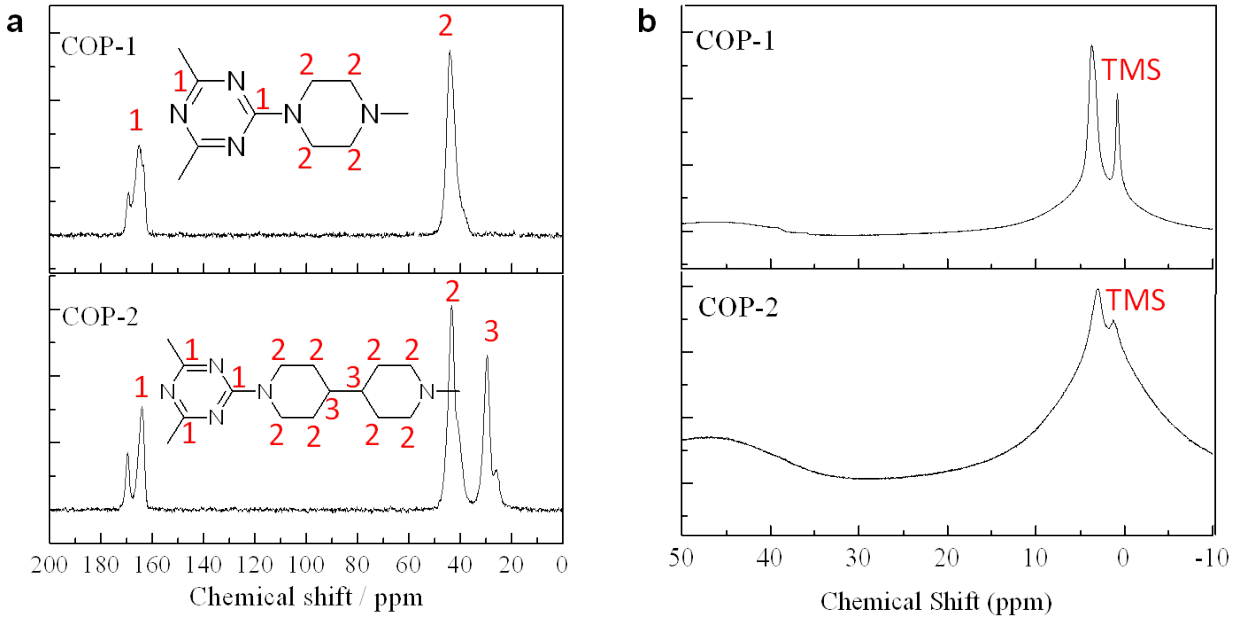

Fig. S4. ^{13}C and ^{1}H-NMR Spectra. Solid state, (**a**) ^{13}C CPMAS NMR spectra, (**b**) ^{1}H-NMR spectra and relative assignments of the respective structures.

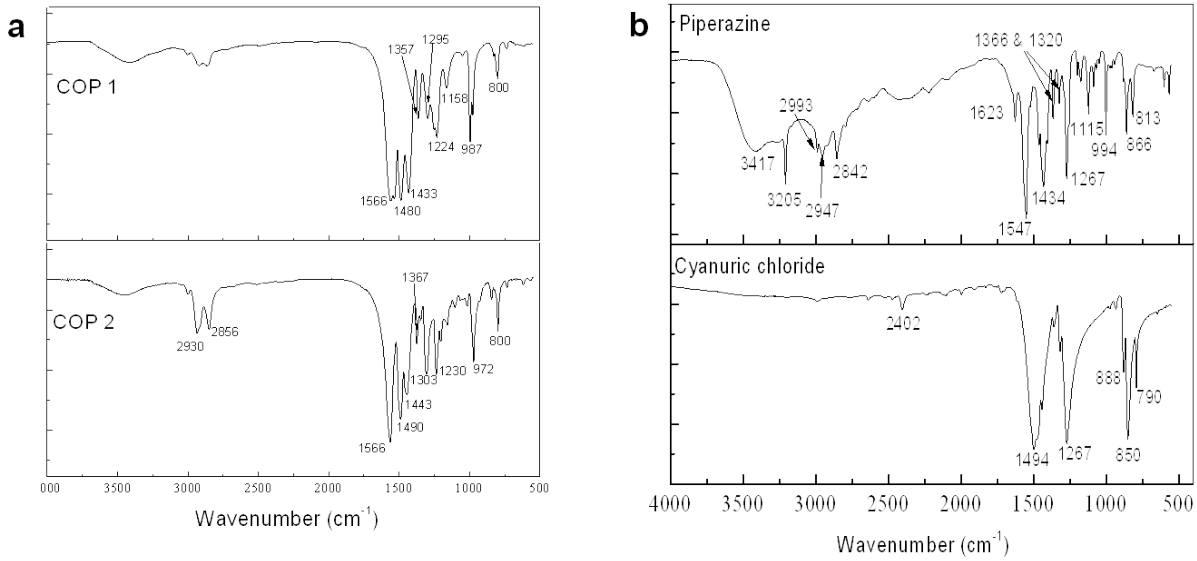

Fig. S5. FT-IR spectra of (**a**) COPs, and (**b**) Cyanuric chloride, piperazine.

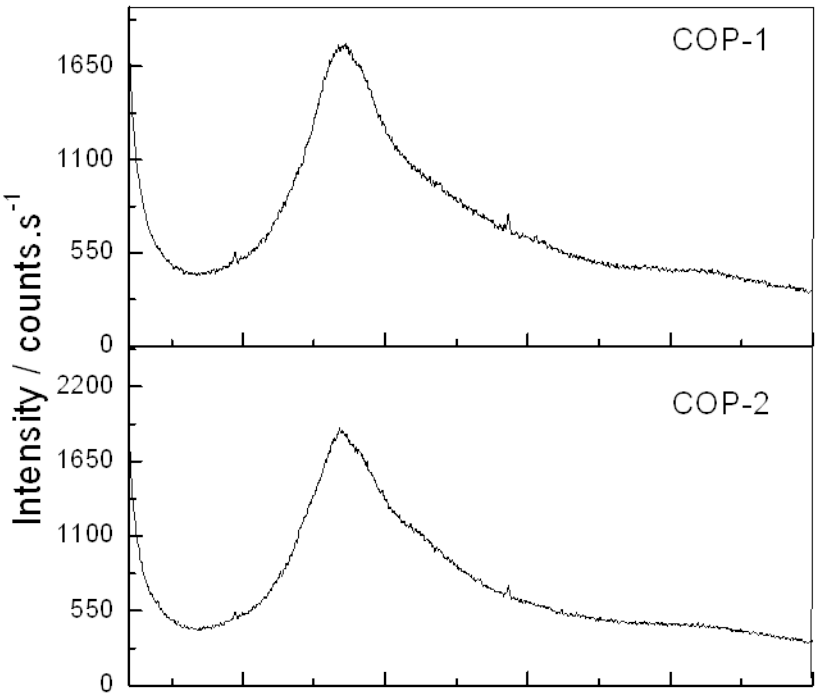

Fig. S6. Powder X-ray diffraction (XRD) patterns of the COPs were acquired from 0.5 to 60° by a Rigaku D/MAX-2500 (18kW) Micro area X-ray diffractometer.

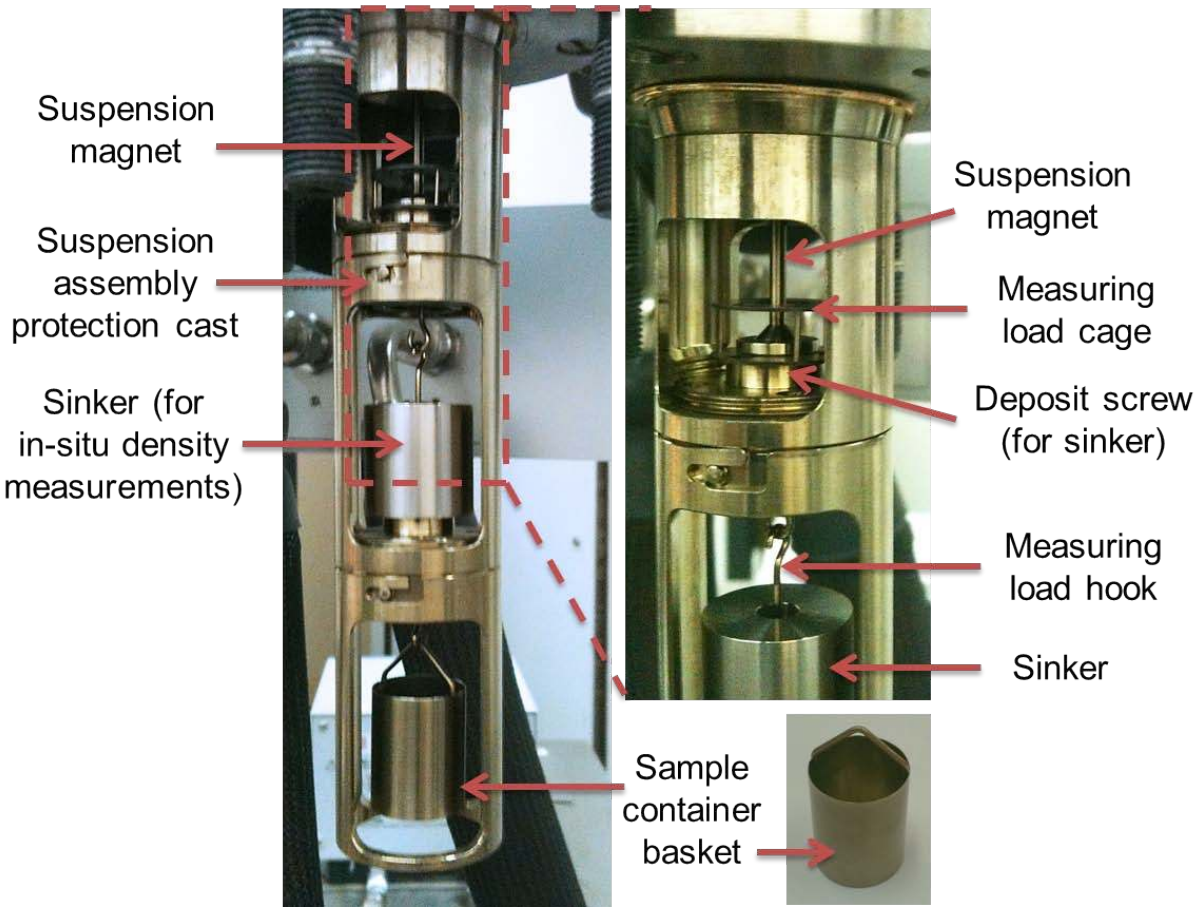

Fig. S7. Rubotherm® Magnetic Suspension Balance (MSB). Photos of the magnetic suspension assembly and the sample container basket.

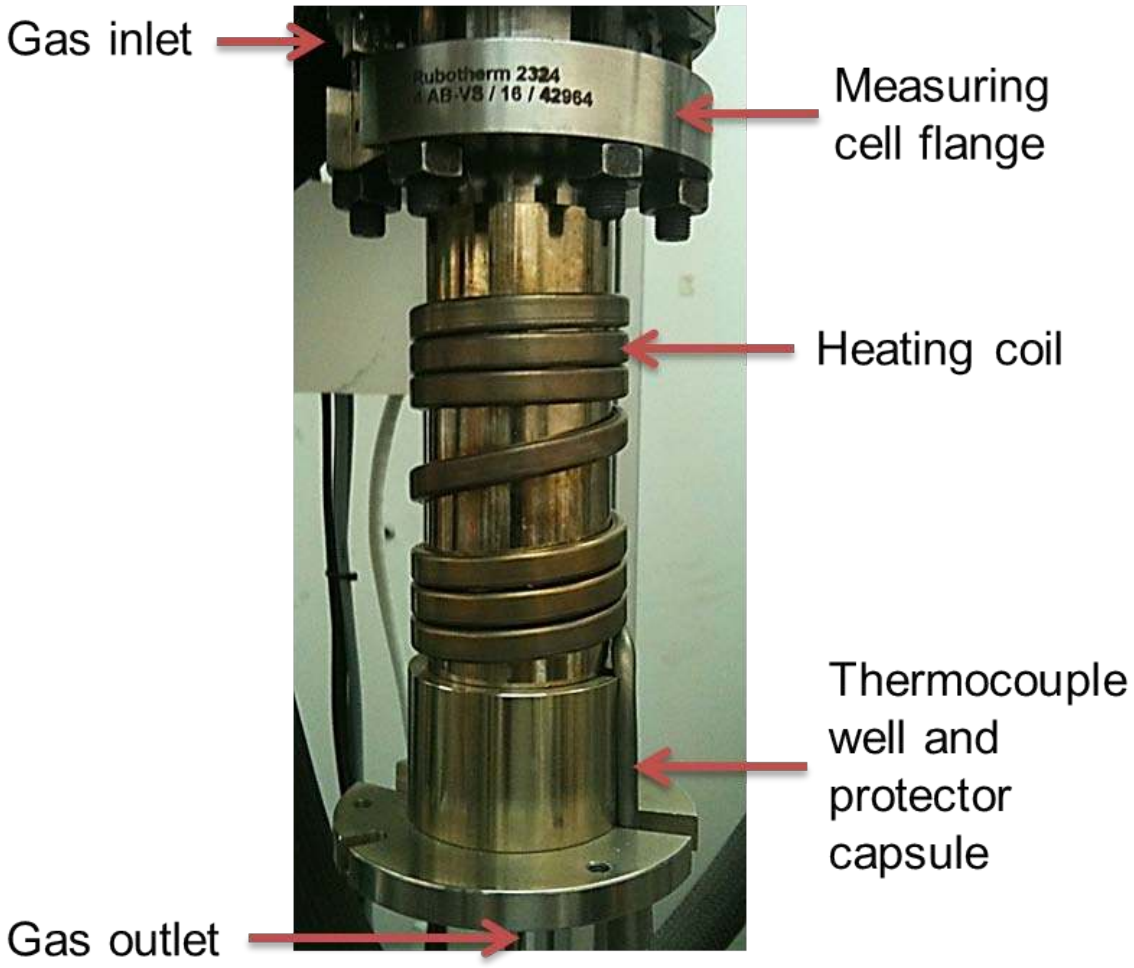

Fig. S8. MSB overview. Photo of the measuring cell and the magnetic coupling housing

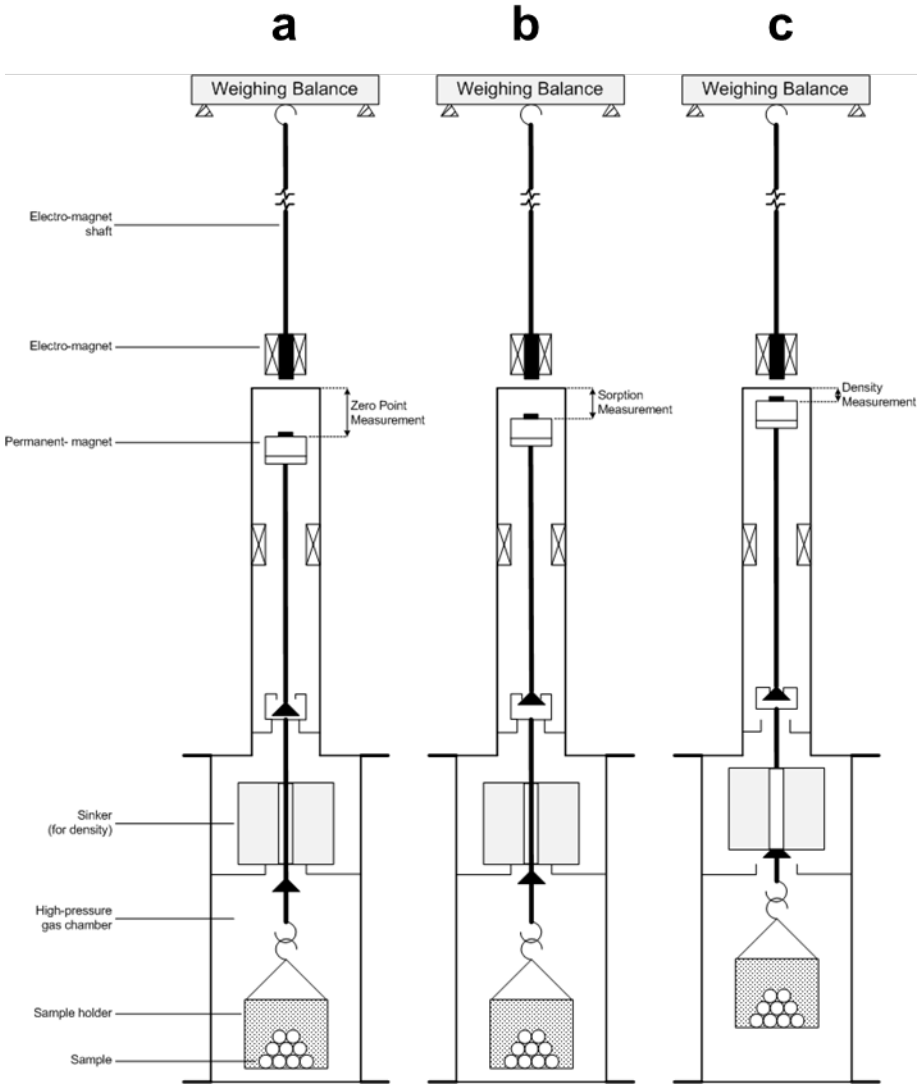

Fig. S9. Schematics of magnetic suspension sorption apparatus operating principle. (**a**) sample loaded to measuring basket in high pressure cell; (**b**) Measurement point 1 (MP1) - magnetic coupling is on and mass of the sample is measured; (**c**) Measurement point 2 (MP2) – in-situ density of the adsorbed gas is measured.

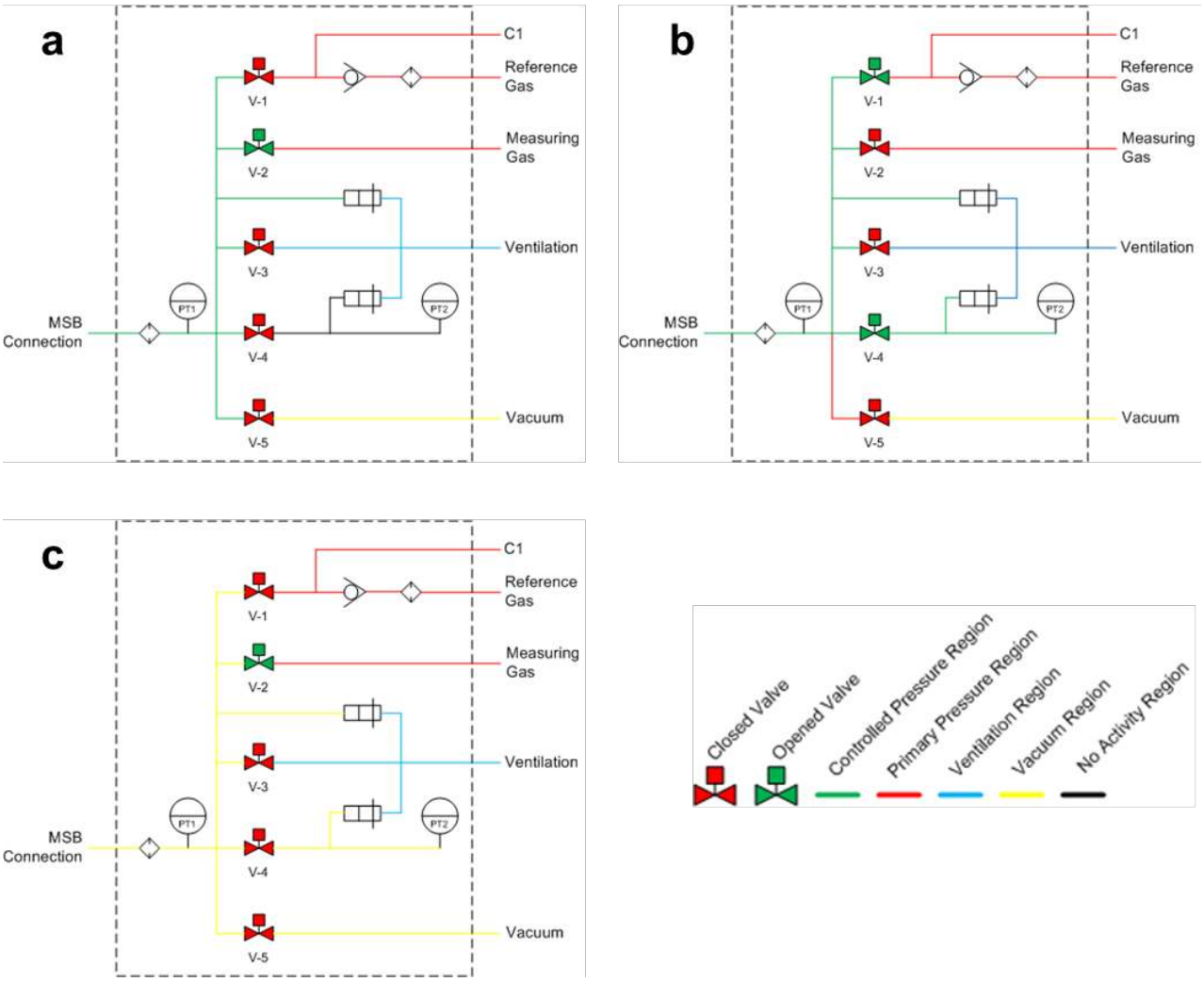

Fig. S10. Schematics of the gas dosing manifold system under (**a**) CO_2 measurement; (**b**) reference gas (He) measurement; (**c**) vacuum measurement

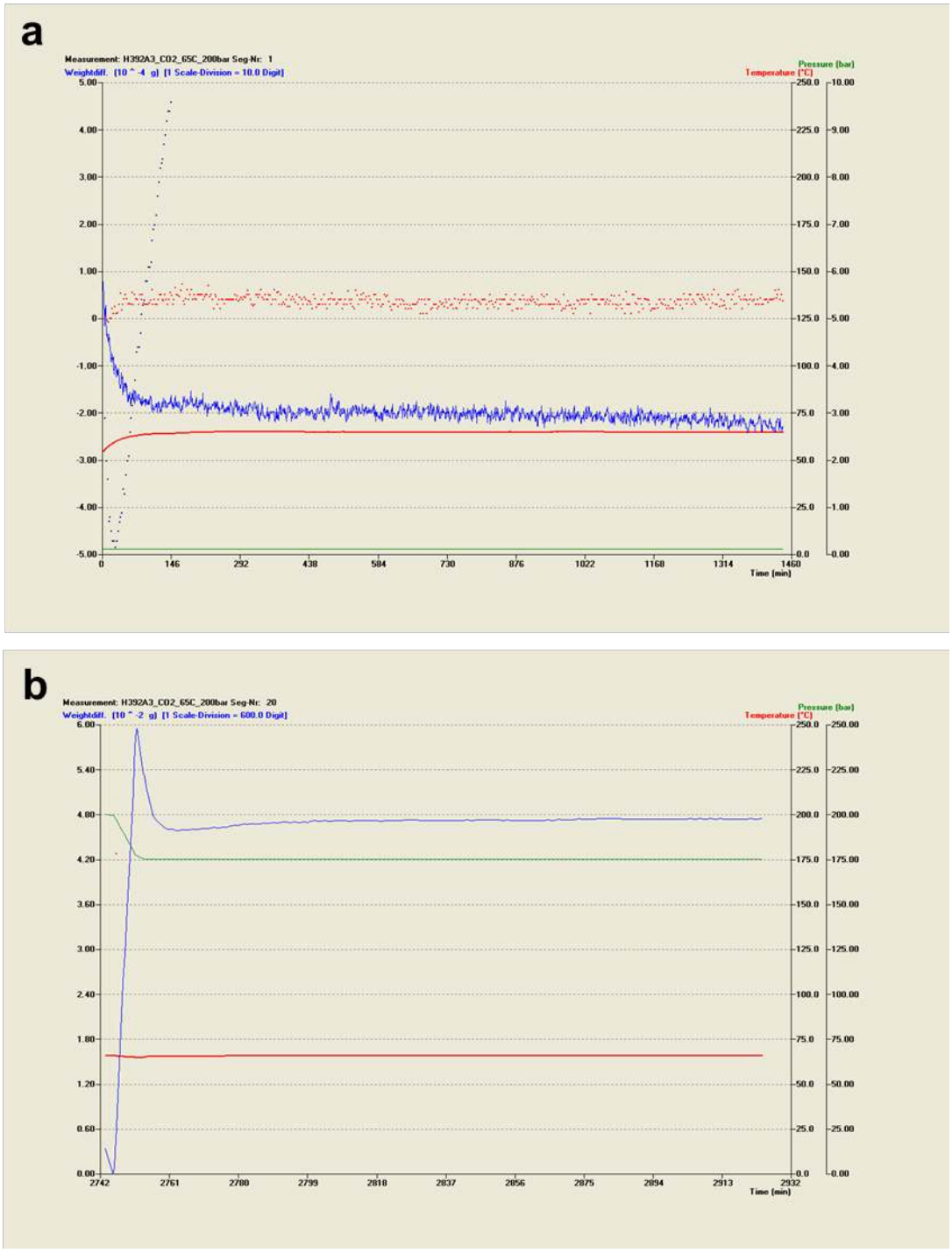

Fig. S11. Magnetic suspension sorption apparatus screenshots at, (**a**) vacuum and, (**b**) under pressure measurement.

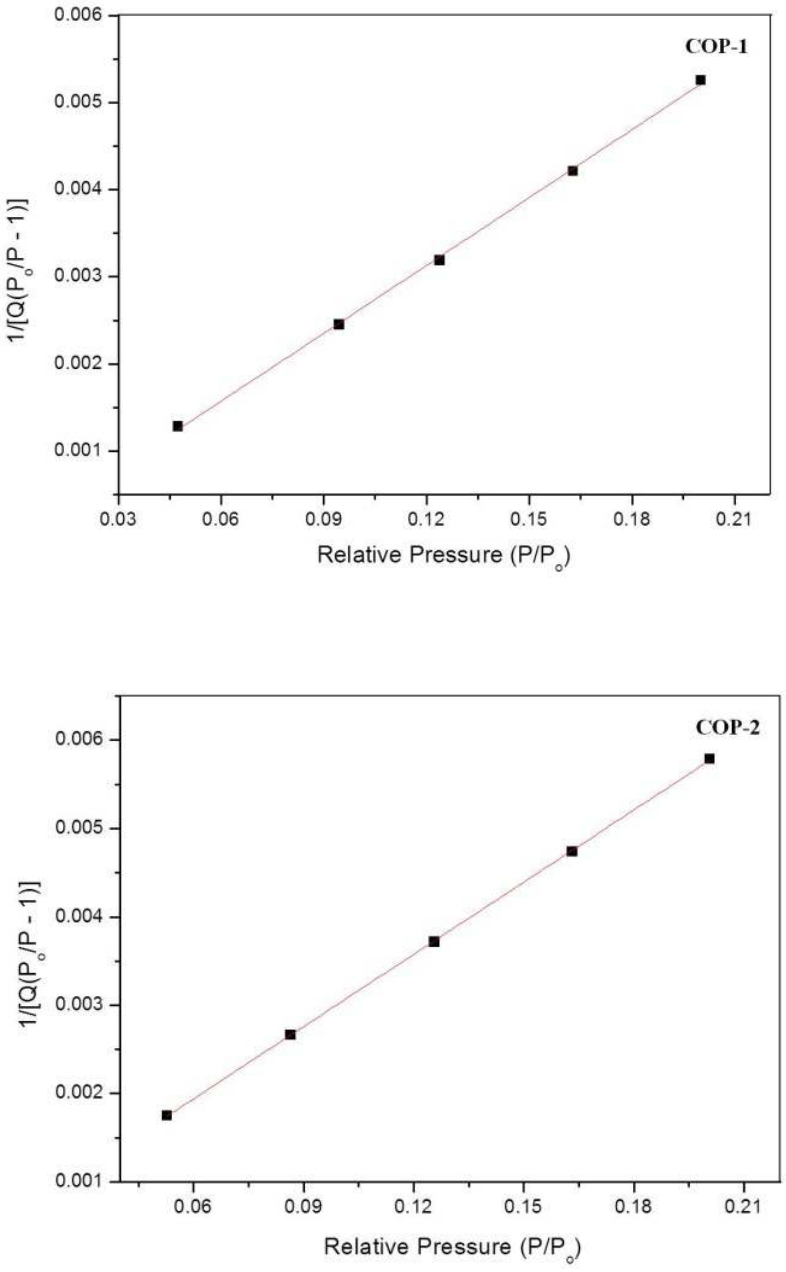

Fig. S12. BET surface area measured within the partial pressure range of 0.05-0.15.

Supplementary Movies

Each GCMC was performed using the sorption module in Cerius2 (Accelrys Software Inc.) and the movies were created using BandiCam (Bandisoft.com).

Below is the list of movies and their descriptions:

Movie S1. Simulation of COP-1 at 20 atm.

Movie S2. Simulation of COP-1 at 50 atm.

D. Supplementary Tables

Table S1. Effect of the synthesis solvent and reaction temperature on the surface area of the COP-1. Reaction time was kept constant since no change was observed after 24h.

Solvent	Surface Area$_{BET}$ $m^2.g^{-1}$	Reaction Temperature, °C	Time, h
Dioxane	168	85	24
Dioxane	66	70	24
THF	70	70	24
Dimethyl Acetamide	43	80	24
Ethanol	1	70	24
Toluene	41	80	24

Table S2. Bulk density and tapped bulk density of COPs.

	Bulk density $g.cm^{-3}$	**Tapped bulk density** $g.cm^{-3}$
COP-1	0.096	0.127
COP-2	0.191	0.253

Table S3. Elemental (C, H, N and S) analysis.

		COP-1	COP-2
%C	Experimental	54.2	64.7
	Theoretical	52.2	64
%H	Experimental	6.2	7.6
	Theoretical	4.4	7.4
%N	Experimental	39.6	27.6
	Theoretical	43.5	28.7
%S	Experimental	-	-
	Theoretical	-	-

Table S4. Detailed analyses of surface area, pore size and volume, and micropore area.

	COP-1	**COP-2**
BET, $m^2.g^{-1}$	168	158
Langmuir, $m^2.g^{-1}$	223	217
Pore size, nm	6.6	17.7
Pore volume, $cm^3.g^{-1}$	0.25	0.67
t-plot micropore area, $m^2.g^{-1}$	67	16

Table S5. CO_2/N_2 selectivities and CO_2 adsorption capacities of COPs per surface area at 1 bar.

COPs	Surface area, BET $m^2.g^{-1}$	CO_2 Adsorption $mg.g^{-1}$	N_2 Adsorption $mg.g^{-1}$	Selectivity CO_2/N_2	CO_2 Adsorption/Surface area $mg.m^{-2}$
COP-1	167	60	2.4	25	0.36
COP-2	158	41	5.2	7.9	0.26

Table S6. Theoretical estimation for geometrical properties and CO_2 uptake of three frames, COP-1, MOF-5, and crystalline COP-1. The latter two structures were added to give contrast to the findings.

Frame	Density / g.cm^{-3}	Porosity		Adsorbed CO_2 mmol.g^{-1}	
		%	cm^3.g^{-1}	10 bar	200 bar
Amorphous COP-1	0.127	85.5	6.7	5.7	119.1
MOF-5	0.589	59.8	1.0	6.4	25.4
Crystalline COP-1	0.954	21.7	0.2	4.1	6.2

Table S7. Numerical values for H_2 adsorption at 298 K. Some of the adsorption values were normalized to 0, when no meaningful data was measured.

Pressure / bar	Adsorbed H_2 / $mg.g^{-1}$	
	COP-1	COP-2
0.04421	0	0
0.55411	0.007	0
1.0382	0.281	0
10.895	0.6	0
20.503	1.157	0
36.014	1.356	0
51.3	1.382	0
66.666	1.715	0
81.845	1.981	0
96.621	2.332	0
108.77	3.082	0

Table S8. Numerical values for CO_2 adsorption at 318 K

Pressure / bar	Adsorbed CO_2 / $mg.g^{-1}$	
	COP-1	COP-2
0.12	2.427977	2.190328
9.961	208.7602	87.25224
19.971	372.2545	159.2963
29.955	538.9743	231.2875
39.955	721.0905	308.5181
49.956	920.4733	392.1739
74.956	1592.083	664.2749
99.953	3178.004	1268.045
124.953	4596.116	1738.647
149.961	5099.608	1909.036
174.966	5398.751	2011.41
199.969	5615.702	2086.281

Table S9. Numerical values for CO_2 adsorption at 328 K

Pressure / bar	Adsorbed CO_2 / mg/g^{-1}	
	COP-1	COP-2
0.12	3.709519	2.557363
9.99	191.5958	78.2783
19.999	346.5612	145.062
29.952	502.8609	212.0389
39.974	671.7569	282.7151
49.958	852.6959	357.5832
74.957	1410.303	582.0886
99.958	2309.816	934.9549
124.957	3652.808	1427.336
149.959	4482.273	1701.626
174.961	4920.276	1849.774
199.968	5212.835	1950.428

Table S10. Numerical values for CO_2 adsorption at 338 K

Pressure / bar	Adsorbed CO_2 / $mg.g^{-1}$	
	COP-1	COP-2
0.12	2.83594	2.927919
9.96	167.9397	63.74748
19.954	312.7456	124.0204
29.955	460.8464	184.7533
39.96	619.057	249.7392
49.956	786.9223	318.5966
74.959	1276.517	514.9379
99.966	1947.555	782.0228
124.957	2889.209	1141.503
149.96	3804.614	1467.141
174.966	4400.062	1670.14
199.969	4787.583	1801.666

E. Supplementary Notes

1. J. G. Harris and K. H. Yung, *Journal of Physical Chemistry*, 1995, **99**, 12021-12024.
2. J. P. Perdew, K. Burke and M. Ernzerhof, *Physical Review Letters*, 1996, **77**, 3865-3868.
3. R. Dawson, A. Laybourn, Y. Z. Khimyak, D. J. Adams and A. I. Cooper, *Macromolecules*, 2010, **43**, 8524-8530.
4. G. Blotny, *Tetrahedron*, 2006, **62**, 9507-9522.
5. R. Kleinrahm and W. Wagner, *Progress Reports of the VDI Journals*, 1984, **3**.
6. H. W. Lösch, *Development and Design of New Magnetic Suspension Balances for Non-Contact Measurements of Vertical Forces*, VDI Verlog, Düsseldorf, 1987.